Energy spectrum of hydrogen atoms in dense plasmas

J. Seidel
Physikalisch-Technische Bundesanstalt, Abbestraße 2-12, 10587 Berlin, Germany

S. Arndt and W. D. Kraeft
Fachbereich Physik, Universität Greifswald, Domstraße 10a, 17487 Greifswald, Germany
(Received 2 February 1995)

From the Bethe-Salpeter equation for the two-particle (proton-electron) Green function, an effective Schrödinger wave equation can be derived for a hydrogen atom in a hydrogen plasma, which describes the perturbation of atomic energy levels and eigenstates by many-particle plasma effects (Pauli blocking, exchange and dynamic self-energy, and interaction-potential correction due to dynamic screening). Taking full account of dynamic screening by the random-phase approximation dielectric function, we solved the effective wave equation for nondegenerate plasmas. For bound atomic states, the plasma effects nearly compensate one another and the energy levels depend only weakly on density. In contrast, the lowering of the continuum edge is not diminished by such compensation, so that the bound states successively merge into the continuum with increasing plasma density. As our results show, reliable calculations have to incorporate dynamic screening, since the use of static screening (which greatly facilitates calculations) may lead to substantial errors, even at low densities.

PACS number(s): 52.20.−j, 52.25.Jm, 05.30.−d

I. INTRODUCTION

Dense (nonideal) plasmas are of scientific and technical interest. We mention dense astrophysical plasmas and experimental investigations in connection with laser or ion beam produced fusion plasmas (see, e.g., [1]). In such plasmas, the mean interaction energy of charged particles may be of the same order as their kinetic energy and we expect that various features deviate esssentially from those of low-density plasmas. In this paper, we focus attention on two-particle properties in dense plasmas and in particular investigate hydrogen atomic states in hydrogen plasmas.

For atoms in a plasma, there are no strictly stationary states. Due to collisions with charged plasma particles (in particular electrons), all atomic states, even the ground state, have a finite lifetime, which depends on plasma density and temperature. This is equivalent to a broadening (or imaginary part) of atomic energy eigenvalues and will in general be accompanied by an energy level shift as well. As one well-known result, spectral lines show plasma (Stark) broadening and may show a shift if the corresponding upper and lower atomic energy levels are shifted by different amounts. We note, however, that "upper-lower state interference" or "vertex contributions" play an additional role in this connection, beside the self-energy corrections of single-particle energies (dressed particles), in particular for hydrogen lines.

For highly exited states, the perturbation by the surrounding plasma will have drastic consequences since states with a radius of the order of the mean interparticle distance will certainly cease to exist as atomic states in a plasma. Thus we expect the continuum edge of the atomic energy spectrum to be lowered in a plasma, as compared to a free unperturbed atom. By this, the energy spectrum of hydrogen atoms, for example, will be reduced to a finite number of levels.

The theoretical treatment of plasma effects on atomic structure is difficult because this is a genuine many-particle problem: Due to the long range of the Coulomb potential, an atom is always under the simultaneous influence of many plasma electrons and ions, which partly shield or screen one another. Thus many-particle theory is required. The work presented here attempts to yield improved results for plasma effects on atomic structure by use of the Green-function method for charged particle systems, which was developed as a powerful tool during the past few decades [2–4].

Previous attempts [5–12] took account of the dynamic character of the shielding of the Coulomb interaction in this connection by using simple or highly refined approximations, but dealt with semiconductor (electron-hole) plasmas and excitonic (instead of atomic) energy levels or optical spectra. Another recent approach [13–16] did deal with hydrogen plasmas and atoms, but was restricted to static Debye screening from the beginning, which greatly simplified the problem. In contrast, the present work is concerned with hydrogen atoms and plasmas and accounts for dynamic screening. With a view to present experimental possibilities, the treatment is confined to nondegenerate plasmas, but this is not an essential limitation.

II. EFFECTIVE HAMILTONIAN

In the framework of the Green-function method [4], properties of bound two-particle states are described by

the two-particle Green function g_{ie}, which is to be determined from the Bethe-Salpeter equation

$$g_{ie}(121'2') = g_i(11')g_e(22') + i\hbar \int d3d4d\bar{3}d\bar{4}\, g_i(13)g_e(24) \times K_{ie}(34\bar{3}\,\bar{4})g_{ie}(\bar{3}\,\bar{4}1'2'). \quad (1)$$

Here 1 is an abbreviation for $(\boldsymbol{r}_1, t_1)$, etc. The one-particle Green functions g_i, g_e are solutions of the Dyson equation. The two-particle Green function is coupled to the three-particle Green function, and so on, so that an infinite hierarchy of equations results. In the Bethe-Salpeter equation (1), this coupling to the higher-order Green functions is hidden in the effective interaction kernel K_{ie}. To decouple the hierarchy, but still retain the most important many-particle effects, we replace the effective interaction by the dynamically screened two-particle potential

$$K_{ie}(34, \bar{3}\,\bar{4}) = V^s_{ie}(34)\delta(3\bar{3})\delta(4\bar{4}). \quad (2)$$

With this approximation, the Bethe-Salpeter equation for g_{ie} yields an effective Schrödinger wave equation for an ion (proton)-electron pair in the plasma.

A. Effective wave equation

The Bethe-Salpeter equation (1) taken in the particle-particle channel ($t_1 = t_2$, $t_1' = t_2'$) is transformed into the momentum-Matsubara representation [2,4] according to

$$g_{ie}(12,1'2') = \frac{1}{(-i\hbar\beta)^2}\sum_{\nu,\nu'}\int \frac{d^3p_1 d^3p_2 d^3p_1' d^3p_2'}{(2\pi\hbar)^{12}} \exp\left[-iz^i_\nu(t_1 - t_1') - iz^e_{\nu'}(t_2 - t_2')\right] \times \exp\left[\frac{i}{\hbar}(\boldsymbol{p}_1\cdot\boldsymbol{r}_1 + \boldsymbol{p}_2\cdot\boldsymbol{r}_2 - \boldsymbol{p}_1'\cdot\boldsymbol{r}_1' - \boldsymbol{p}_2'\cdot\boldsymbol{r}_2')\right] g_{ie}(\boldsymbol{p}_1,\boldsymbol{p}_2,\boldsymbol{p}_1',\boldsymbol{p}_2',z^i_\nu,z^e_{\nu'}), \quad (3)$$

for instance [$z^a_\nu = i\pi\nu/(\hbar\beta) + \mu_a$, ν is odd, μ_a is the chemical potential, $a = i, e$, and $\beta = 1/(k_B T)$]. Then, the sums over the Matsubara frequencies are performed and the frequency-dependent functions are continued into the complex plane. In the course of this, the two-frequency Green function is replaced by a single-frequency Green function by means of the Shindo approximation [17–19]

$$g_{ie}(\boldsymbol{p}_1 - \boldsymbol{q}, \boldsymbol{p}_2 + \boldsymbol{q}, \boldsymbol{p}_3, \boldsymbol{p}_4, z^i_\nu, \Omega^{ie}_\lambda - z^i_\nu) = \frac{-i\hbar\beta\left[g_i(\boldsymbol{p}_1 - \boldsymbol{q}, z^i_\nu) + g_e(\boldsymbol{p}_2 + \boldsymbol{q}, \Omega^{ie}_\lambda - z^i_\nu)\right]}{\sum_{\nu'}\left[g_i(\boldsymbol{p}_1 - \boldsymbol{q}, z^i_{\nu'}) + g_e(\boldsymbol{p}_2 + \boldsymbol{q}, \Omega^{ie}_\lambda - z^i_{\nu'})\right]} \times g_{ie}(\boldsymbol{p}_1 - \boldsymbol{q}, \boldsymbol{p}_2 + \boldsymbol{q}, \boldsymbol{p}_3, \boldsymbol{p}_4, \Omega^{ie}_\lambda) \quad (4)$$

[$\Omega^{ie}_\lambda = i\pi\lambda/(\hbar\beta) + \mu_i + \mu_e = z^i_\nu + z^e_{\nu'}$, λ even]. This is exact for static potentials V^s_{ie} only, while its usefulness for dynamic screening is uncertain and, most probably, limited to weak retardation effects. Use of the Shindo approximation at this point in the calculation is common practice in all the work done in the field, but it is certainly a possible source of error.

The Hermitian part of the resulting homogeneous Bethe-Salpeter equation is the effective Schrödinger wave equation for the wave function Ψ of an ion-electron pair in the many-particle system [4,20], which provides the starting point of our work:

$$[H_{ie}(\boldsymbol{p}_i, \boldsymbol{p}_e, \omega) - \hbar\omega]\,\Psi(\boldsymbol{p}_i, \boldsymbol{p}_e, \omega) = 0, \quad (5)$$

$$H_{ie}(\boldsymbol{p}_i, \boldsymbol{p}_e, \omega) = H^{(0)}_{ie}(\boldsymbol{p}_i, \boldsymbol{p}_e) + \mathrm{Re}\, H^{\mathrm{pl}}_{ie}(\boldsymbol{p}_i, \boldsymbol{p}_e, \omega + i0).$$

$H^{(0)}_{ie}$ is the Hamiltonian of the isolated two-particle Coulomb problem, while $\mathrm{Re}\, H^{\mathrm{pl}}_{ie}$, the real part of the plasma Hamiltonian, which occurs in the inhomogeneous Bethe-Salpeter equation, describes the influence of the surrounding plasma on the two-particle complex. As a consequence of dynamic screening, the plasma Hamiltonian depends on ω and is different for different energy eigenvalues $E = \hbar\omega$, so that Eq. (5) is not just an eigenvalue problem, but has to be solved self-consistently with respect to ω. The solutions of the effective Schrödinger equation determine the two-particle Green function g_{ie}, the real eigenvalues corresponding to δ-like singularities of the two-particle spectral function [20].

Here we consider the wave equation for an atom at rest (vanishing total momentum) in a nondegenerate plasma. In addition, we restrict plasma effects to the lowest order of plasma density by neglecting all higher-order terms except those that occur through the dielectric function. With these approximations, the effective wave equation for an atom in a plasma becomes [4]

$$\left(\frac{p^2}{2m_{ie}} - \hbar\omega\right)\psi(\boldsymbol{p},\omega) + \int \frac{d^3q}{(2\pi\hbar)^3} V^{\mathrm{C}}_{ie}(q)\psi(\boldsymbol{p}+\boldsymbol{q},\omega) = \int \frac{d^3q}{(2\pi\hbar)^3} V^{\mathrm{C}}_{ie}(q)\left\{[f_i(\boldsymbol{p}) + f_e(\boldsymbol{p})]\,\psi(\boldsymbol{p}+\boldsymbol{q},\omega) - [f_i(\boldsymbol{p}+\boldsymbol{q}) + f_e(\boldsymbol{p}+\boldsymbol{q})]\,\psi(\boldsymbol{p},\omega)\right\} + \int \frac{d^3q}{(2\pi\hbar)^3}\Delta V^{\mathrm{eff}}_{ie}(\boldsymbol{q},\boldsymbol{p},\omega)\,[\psi(\boldsymbol{p}+\boldsymbol{q},\omega) - \psi(\boldsymbol{p},\omega)] \quad (6)$$

with the effective potential correction

$$\Delta V_{ie}^{\rm eff}(\boldsymbol{q},\boldsymbol{p},\omega) = \mathrm{P}\int_{-\infty}^{\infty}\frac{d(\hbar\omega')}{\pi}\mathrm{Im}\,V_{ie}^{s}(q,\omega') \times\left[\frac{n_{\rm B}(\omega')+1}{\hbar(\omega-\omega')-E_i(\boldsymbol{p})-E_e(\boldsymbol{p}+\boldsymbol{q})} +\frac{n_{\rm B}(\omega')+1}{\hbar(\omega-\omega')-E_i(\boldsymbol{p}+\boldsymbol{q})-E_e(\boldsymbol{p})}\right], \quad (7)$$

given by a principal value integral, the Bose function $n_{\rm B}(\omega)=(e^{\beta\hbar\omega}-1)^{-1}$, and the Fermi functions f_i and f_e, which become Maxwell-Boltzmann distributions (proportional to the plasma density $n_e=n_i$) for nondegenerate plasmas. The wave function ψ relates to relative motion and m_{ie} is the reduced mass of the ion-electron pair. The quasiparticle energies of electrons and ions E_e and E_i are discussed in more detail in Sec. II B. The connection of the plasma-screened potential V_{ie}^{s}, Eq. (2), with the "bare" Coulomb potential $V_{ie}^{\rm C}$ is given by the retarded (longitudinal) dielectric function $\varepsilon(k,\omega)=\varepsilon(k,\omega+i0)$, which is traditionally expressed as a function of a wave vector, not a momentum:

$$V_{ie}^{s}(q,\omega)=\frac{V_{ie}^{\rm C}(q)}{\varepsilon(q/\hbar,\omega)}. \quad (8)$$

The approximations we used for the dielectric function are specified in Sec. II C.

In Eq. (6), the many-body effects are contained on the right-hand side (rhs), which is proportional to the plasma density in the low-density limit (via f_i, f_e, and $\mathrm{Im}\varepsilon^{-1}$), so that the usual Schrödinger wave equation for the unperturbed Coulomb problem is recovered for vanishing plasma density. There are four different kinds of many-body effects: general many-particle effects (first integral on the rhs); namely, phase space occupation (Pauli blocking) and exchange (Hartree-Fock) self-energy; and effects connected with the plasma screening of the Coulomb potential (second integral); namely, the dynamically screened effective potential correction and dynamic (Montroll-Ward) self-energy. We note that the effective potential correction $\Delta V_{ie}^{\rm eff}$ given by Eq. (7) is more complicated than $V_{ie}^{s}-V_{ie}^{\rm C}$.

The effective wave equation (5) or (6) yields real energy eigenvalues $E=\hbar\omega$, because it corresponds to the "real" Hermitian part of the homogeneous Bethe-Salpeter equation. The imaginary parts Γ of the energy eigenvalues are determined by perturbation theory (Sec. II E).

B. Single-particle self-energies and the two-particle continuum edge

The single-particle energies in the potential correction Eq. (7) for the effective Schrödinger equation (6) are quasiparticle energies. They differ by the single-particle self-energies from the kinetic energies of free particles and are self-consistent solutions of

$$E_a(\boldsymbol{p})=\frac{p^2}{2m_a}+\Sigma_a[p,\omega=E_a(\boldsymbol{p})/\hbar],\quad a=i,e. \quad (9)$$

In correspondence with the approximation we made for the effective interaction K_{ie} in Eq. (2), we also neglect the vertex corrections for the self-energy [4]. This leads to the V^s approximation

$$\Sigma_a(12)=i\hbar V_{aa}^{s}(12)g_a(12). \quad (10)$$

The additional Hartree contribution found in the general case vanishes for an electrically neutral plasma [4]. After transformation into the momentum-Matsubara representation and continuation into the complex frequency plane, the single-particle self-energy becomes

$$\Sigma_a(p,\omega)=\Sigma_a^{\rm HF}(p)+\mathrm{P}\int\frac{d^3q\,d(\hbar\omega)}{(2\pi\hbar)^3\,\pi}\mathrm{Im}\,V_{aa}^{s}(q,\omega') \times\frac{1+n_{\rm B}(\omega')-f_a(\boldsymbol{p}+\boldsymbol{q})}{\hbar(\omega-\omega')-E_a(\boldsymbol{p}+\boldsymbol{q})}. \quad (11)$$

The second term is usually referred to as the Montroll-Ward contribution. In our calculation, the Fermi function in the nominator is neglected because $f_a\mathrm{Im}\varepsilon^{-1}$ is second order in the density. The first term is the Hartree-Fock contribution

$$\Sigma_a^{\rm HF}(p)=-\int\frac{d^3q}{(2\pi\hbar)^3}V_{aa}^{\rm C}(q)f_a(\boldsymbol{p}+\boldsymbol{q}) =-\frac{2\pi\hbar^2e_a^2n_a\beta}{4\pi\varepsilon_0m_a}\,{}_1F_1\left(1,\frac{3}{2},-\frac{\beta p^2}{2m_a}\right), \quad (12)$$

the last expression being valid in the nondegenerate case.

As far as we know, self-consistent solutions of the strongly nonlinear integral equation (9) are not available for the case of large ion-electron mass ratios m_i/m_e, and we did not succeed in finding such a solution in the work reported here either. However, as long as we are concerned with the plasma effects on hydrogenic bound states in only the lowest order of plasma density, this is not a serious problem.

The electron and ion self-energies vanish for vanishing plasma density. If they were included in the quasiparticle energies in the resonance denominators of the potential correction Eq. (7), they would give rise to density-dependent contributions to this quantity. But $\mathrm{Im}\varepsilon^{-1}$ in the nominator is already of first order in the density, so these are corrections of higher density order and it would not be consistent to retain them because other terms beyond first order of density are neglected in the effective Schrödinger equation (6). Therefore, we took the quasiparticle energies E_i, E_e to be the kinetic energies in Eq. (7). For the same reason, the energy $\hbar\omega$ in Eq. (7), which should strictly be obtained by self-consistent solution of the effective Schrödinger equation (6), is taken as unperturbed atomic energy eigenvalue $E_n^{\rm C}$ of the Coulomb problem. We note that this facilitates the numerical evaluation because the continuous dependence of the effective Hamiltonian on ω is replaced by a "step function."

The arguments given above apply to bound states with $E_n^{\rm C}\neq 0$. For the continuum edge, with unperturbed eigenvalue $E_\infty^{\rm C}=E_{\rm cont}^{\rm C}=0$, things may be (and in fact

are) different. To determine the position of the continuum edge, we insert the asymptotic wave function of scattering states $\psi(\boldsymbol{p}) \to (2\pi\hbar)^3\delta(\boldsymbol{p})$ into the effective wave equation (6) and obtain

$$E_{\rm cont} = E_i(\boldsymbol{p}=\boldsymbol{0}) + E_e(\boldsymbol{p}=\boldsymbol{0}), \tag{13}$$

where the quasiparticle energies reduce to the self-energies for vanishing momentum $p = 0$. We emphasize that the derivation of this result requires the quasiparticle energies to be exact solutions of Eq. (9). Even if they are only needed for $p = 0$ in Eq. (13), their strict determination requires the self-consistent solution of Eq. (9) for all momenta, due to the appearance of $E_a(\boldsymbol{p}+\boldsymbol{q})$ in the resonance denominator of the integrand of Eq. (11).

Since the single-particle self-energies are not known, as stated above, the continuum edge can only be determined approximatively. Combining Eqs. (9), (11), and (13) yields an equation for $E_{\rm cont}$ that is suitable as a starting point to derive approximations

$$\begin{aligned} E_{\rm cont} = {} & \Sigma_i^{\rm HF}(0) + \Sigma_e^{\rm HF}(0) \\ & + {\rm P}\int \frac{d^3q\, d(\hbar\omega)}{(2\pi\hbar)^3\,\pi} \\ & \times {\rm Im}\, V_{ie}^s(q,\omega)\left[\frac{n_{\rm B}(\omega)+1}{E_{\rm cont}-\hbar\omega-E_i(\boldsymbol{0})-E_e(\boldsymbol{q})}\right. \\ & \left. + \frac{n_{\rm B}(\omega)+1}{E_{\rm cont}-\hbar\omega-E_i(\boldsymbol{q})-E_e(\boldsymbol{0})}\right]. \end{aligned} \tag{14}$$

At first sight, it would seem fully consistent with the approximations used for the bound states to simply neglect the self-energy contributions to the quasiparticle energies in this equation and to replace $E_{\rm cont}$ by its unperturbed value of 0 in the resonance denominators of the rhs, which amounts to the use of the well-known approximation [4]

$$E_a(\boldsymbol{p}) \approx \frac{p^2}{2m_a} + \Sigma_a\left(p, \frac{p^2}{2m_a\hbar}\right) \tag{15}$$

in Eq. (13). However, this does not produce a realistic dependence of the hydrogen atom continuum edge on the plasma density because the results predict, for instance, that none of the Balmer spectral lines would be observable at arc plasma densities because the upper states would already be continuum states, i.e., the continuum edge decreases much too fast with increasing plasma density. Analytical results, which are available for small momentum to the lowest orders of $\hbar$ [4], indicate that this steep decrease of the continuum edge is a particular problem for large values of m_i/m_e.

Therefore, it is necessary to employ an improved approximation. In our work, we stuck to the approximation of $E_a(\boldsymbol{p})$ by the kinetic energy $p^2/(2m_a)$ in Eq. (14), but solved the equation for $E_{\rm cont}$ by iteration. As a result, the steep decrease of the continuum edge with increasing density (at fixed temperature) is drastically reduced and the values obtained in this way are close to the values we can determine from the behavior of the bound states at certain discrete plasma densities; cf. Sec. IV B. We take this as an indication that the additional effects that are brought about by the self-energy contribution to the quasiparticle energy will not be too important in this connection. Nevertheless, a truly consistent treatment has to include both effects since we expect Σ_i and Σ_e as well as $E_{\rm cont}$ to be proportional to $\sqrt{n_e}$ at low plasma density. Further investigation of the single-particle self-energies (in particular of the electronic self-energy for large ion-electron mass ratio) is required for this purpose.

C. Dielectric function

Important plasma effects in the effective wave equation (7) are connected with the dielectric function. In terms of the polarization function Π, the dielectric function is

$$\begin{aligned} \varepsilon(k,\omega) = 1 + \sum_{a,b}\int \frac{d^3p\, d^3q}{(2\pi\hbar)^6}\, V_{ab}^{\rm C}(\hbar k) \\ \times \Pi_{ab}(\boldsymbol{p}-\hbar\boldsymbol{k}, \boldsymbol{q}+\hbar\boldsymbol{k}, \boldsymbol{p}, \boldsymbol{q}, \omega + i0), \end{aligned} \tag{16}$$

where $\boldsymbol{k}$ is a wave vector (not a momentum). We used the polarization function in the random-phase approximation (RPA),

$$\Pi_{ab}^{\rm RPA}(1234) = -\delta_{ab} g_a(14) g_b(23), \tag{17}$$

which again amounts to the neglect of vertex corrections. The corresponding RPA dielectric function is

$$\varepsilon\left(\frac{p}{\hbar},\omega\right) = 1 + \sum_{a=i,e}\int \frac{d^3q}{(2\pi\hbar)^3}\, \frac{V_{aa}^{\rm C}(p)\,[f_a(\boldsymbol{q}) - f_a(\boldsymbol{p}+\boldsymbol{q})]}{E_a(\boldsymbol{q}) - E_a(\boldsymbol{p}+\boldsymbol{q}) + \hbar\omega + i0}. \tag{18}$$

Since we always refer to the RPA dielectric function (or limits of it) here, the corresponding index on ε is omitted. For nondegenerate plasmas, evaluation of the integral is possible [21] and yields the "full" dynamic dielectric function

$$\begin{aligned} \varepsilon(k,\omega) = 1 - i\frac{\sqrt{\pi}}{4}\frac{\kappa^2}{k^2}\left[\frac{w(x+y) - w(x-y)}{2y}\right. \\ \left. + \frac{w(sx+y/s) - w(sx-y/s)}{2y/s}\right] \end{aligned} \tag{19}$$

with

$$x = \frac{1}{2}\frac{\omega/\omega_e}{k/\kappa}, \quad y = \sqrt{\frac{\hbar^2k^2\beta}{8m_e}}, \quad s = \sqrt{\frac{m_i}{m_e}},$$

$$\kappa = 1/r_{\rm D} = \sqrt{2n_e e^2\beta/\varepsilon_0}, \quad \omega_e = \sqrt{e^2n_e/(\varepsilon_0 m_e)},$$

$r_{\rm D}$ being the Debye length and ω_e the electron plasma frequency. The function w is closely related to the complex error function [22]

$$w(z) = \exp(-z^2)\,{\rm erfc}(-iz). \tag{20}$$

For real argument x, its real part is ${\rm Re}w(x) = \exp(-x^2)$ and its imaginary part can be expressed in terms of Daw-

son's integral F or the confluent hypergeometric function ${}_1F_1$ as

$$\frac{\sqrt{\pi}}{2}\mathrm{Im}\, w(x)=\int_0^x dt\, e^{t^2-x^2}=F(x)=x\,{}_1F_1(1,\tfrac{3}{2};-x^2). \tag{21}$$

In the limit $\hbar\to 0$, i.e., $y\to 0$ in Eq. (19), the full dielectric function becomes the "classical" dielectric function

$$\varepsilon_{\mathrm{cl}}(k,\omega)=1+\frac{\kappa^2}{k^2}\left\{1+i\frac{\sqrt{\pi}}{2}\left[xw(x)-sxw(sx)\right]\right\}. \tag{22}$$

The static limit $\omega\to 0$, i.e., $x\to 0$ in Eq. (19), of the full dielectric function is

$$\varepsilon_{\mathrm{st}}(k)=\varepsilon(k,0)=1+\frac{\kappa^2}{k^2}\frac{1}{2}\left[\frac{F(y)}{y}+\frac{F(y/s)}{y/s}\right], \tag{23}$$

while the static limit of the classical dielectric function ($\hbar\to 0$, $\omega\to 0$) is the "Debye limit"

$$\varepsilon_{\mathrm{D}}(k)=\varepsilon_{\mathrm{cl}}(k,0)=1+(\kappa/k)^2. \tag{24}$$

For both $\varepsilon_{\mathrm{st}}$ and ε_{D} the imaginary parts vanish. Note that the static full dielectric function does not lead to Debye screening, but contains additional quantum corrections.

D. Static limit

In the static limit, the screened potential and the self-energies do not depend on frequency and the problems discussed in Sec. II B are absent. In particular, the effective Hamiltonian does not depend on the energy eigenvalue to be determined. In addition, the Shindo approximation Eq. (4) is exact. Repeating the steps that lead from the Bethe-Salpeter equation (1) to Eqs. (6) and (7) with a statically screened potential V_{ie}^s in the effective interaction kernel K_{ie}, Eq. (2), gives the static effective potential correction as

$$\Delta V_{ie}^{\mathrm{eff}}(\boldsymbol{q},\boldsymbol{p})=\left[1-f_i(\boldsymbol{p})-f_e(\boldsymbol{p})\right]\left[V_{ie}^s(q)-V_{ie}^{\mathrm{C}}(q)\right], \tag{25}$$

and results in a simplified effective wave equation. In the Debye limit, for instance, it becomes (V_{ie}^{D} Debye potential)

$$\begin{aligned}\hbar\omega\,\psi(\boldsymbol{p})=&\left[\frac{p^2}{2m_{ie}}+\Sigma_i^{\mathrm{HF}}(p)+\Sigma_e^{\mathrm{HF}}(p)-\frac{e^2\kappa}{4\pi\varepsilon_0}\right]\psi(\boldsymbol{p})\\&+\left[1-f_i(\boldsymbol{p})-f_e(\boldsymbol{p})\right]\int\frac{d^3q}{(2\pi\hbar)^3}V_{ie}^{\mathrm{C}}(q)\psi(\boldsymbol{p}+\boldsymbol{q})\\&+\int\frac{d^3q}{(2\pi\hbar)^3}\left[V_{ie}^{\mathrm{D}}(q)-V_{ie}^{\mathrm{C}}(q)\right]\psi(\boldsymbol{p}+\boldsymbol{q}).\end{aligned} \tag{26}$$

The result for the continuum edge in the Debye limit is

$$\hbar\omega_{\mathrm{cont}}^{\mathrm{D}}=\Sigma_i^{\mathrm{HF}}(p=0)+\Sigma_e^{\mathrm{HF}}(p=0)-\frac{e^2\kappa}{4\pi\varepsilon_0}. \tag{27}$$

The last term is the shift of the continuum edge proposed by Ecker and Weizel [23].

E. Imaginary parts

As noted above, the effective wave equation (6) has real energy eigenvalues because only the Hermitian part of the plasma Hamiltonian is included and the "imaginary" non-Hermitian part is neglected. This is not a serious shortcoming however: If an approximate two-particle description of an ion-electron pair in a plasma is to be sensible at all, its lifetime must not be too short, i.e., the imaginary parts of its energy eigenvalues must be small. But then a perturbation calculation of the imaginary parts is adequate.

For the imaginary part of the plasma Hamiltonian [4], which corresponds to the effective potential correction Eq. (7), we find

$$\begin{aligned}\mathrm{Im}\, H_{ie}^{\mathrm{pl}}(\boldsymbol{q},\boldsymbol{p},\omega)=&\int d^3q'[\delta(\boldsymbol{q})-\delta(\boldsymbol{q}'-\boldsymbol{q})][(n_{\mathrm{B}}\{\omega-[E_i(\boldsymbol{p})+E_e(\boldsymbol{p}+\boldsymbol{q}')]/\hbar\}+1)\\&\times\mathrm{Im}\, V_{ie}^s[q',\omega-E_i(\boldsymbol{p})/\hbar-E_e(\boldsymbol{p}+\boldsymbol{q}')/\hbar]+(n_{\mathrm{B}}\{\omega-[E_i(\boldsymbol{p}+\boldsymbol{q}')+E_e(\boldsymbol{p})]/\hbar\}+1)\\&\times\mathrm{Im}\, V_{ie}^s[q',\omega-E_i(\boldsymbol{p}+\boldsymbol{q}')/\hbar-E_e(\boldsymbol{p})/\hbar]].\end{aligned} \tag{28}$$

In our work, the imaginary part Γ of a bound state energy that has the real part $E=\hbar\omega$ is calculated as mean value of this operator for the corresponding eigenstate of the Hermitian effective Hamiltonian [the solution of the effective wave equation (6)]

$$\begin{aligned}\Gamma&=\langle\,\psi\,|\,\mathrm{Im}\, H_{\mathrm{ie}}^{\mathrm{pl}}\,|\,\psi\,\rangle\\&=\int\frac{d^3pd^3q}{(2\pi\hbar)^6}\,\psi^*(\boldsymbol{p})\,\mathrm{Im}\, H_{ie}^{\mathrm{pl}}(\boldsymbol{q},\boldsymbol{p},\omega)\psi(\boldsymbol{p}+\boldsymbol{q}).\end{aligned} \tag{29}$$

III. APPROXIMATE SOLUTION OF THE EFFECTIVE WAVE EQUATION

A. Expansion in Coulomb eigenfunctions

The effective wave equation (6) refers to an atom at rest (vanishing total momentum) surrounded by an unbounded equilibrium plasma, without externally applied fields. Accordingly, the atomic effective Hamiltonian is invariant under rotation and its eigenfunctions can be chosen as angular momentum eigenfunctions ψ_{nlm}, as for any system with spherical symmetry. These wave functions can be expanded as

$$\psi_{nlm}(\boldsymbol{p}) = \sum_{n'} c_{n,n'}^{(l,m)} \, \psi^{\mathrm{C}}_{n'lm}(\boldsymbol{p}) \tag{30}$$

in the Hilbert space basis of spherical Coulomb wave functions $\psi^{\mathrm{C}}_{n'lm}$ of the unperturbed hydrogen atom. The Coulomb eigenfunctions in momentum representation are the usual spherical harmonics times a "radial" part, which can be expressed in terms of Gegenbauer's ultraspherical polynomials [24]. We note that the perturbed energy eigenvalues $\hbar\omega_{nl}$ will no longer be degenerate with respect to l, since the "accidental" degeneracy of the Coulomb problem is removed by the many-body effects.

For an atom at rest, there is no mixing of different l and m by the spherically symmetrical plasma Hamiltonian. For a moving atom, for which the total atomic momentum $\boldsymbol{P}$ defines a distinguished direction in space, the situation is considerably more complicated because l mixing occurs and the effective atomic Hamiltonian depends on the magnitude of P. Therefore, our work is restricted to $P = 0$ like all previous calculations we know.

To be exact, the sum in Eq. (30) has to extend to $n' = \infty$ and, in addition, has to include an integral over the unperturbed continuum states. In numerical calculations, only a truncated basis with a finite subset of basis functions can be processed. The choice of the truncated basis is critical because it must be appropriate for the function to be approximately expanded (considering, e.g., symmetry or other general properties). In our work, we restricted the sum in Eq. (30) to the N lowest unperturbed energy levels and completely neglegted the continuum integral. To make sure that the results presented here are not afflicted by this truncation, we did calculations, for representative plasma temperatures and densities, for values of N up to 30 (and even up to 50 for the static cases). For the ground and first few excited states (n = 1,2,3), $N = 10$ turned out to be sufficiently large for the determination of the perturbed energy eigenvalues, even if these are close to the (lowered) continuum edge at higher densities. Still, the complete neglect of all unperturbed continuum state contributions to ψ_{nlm} may be suspected to be risky near the continuum edge. This question is discussed in more detail in Sec. III B.

In the truncated basis of Coulomb eigenstates, the Hamiltonian is represented by a finite-dimensional $N \times N$ matrix with N energy eigenvalues and corresponding eigenstates. Due to the replacement of $\hbar\omega$ by the Coulomb eigenvalue E_n^{C} in the plasma Hamiltonian used for the determination of ψ_{nlm} with dynamic screening (cf. Sec. II B above), the effective Hamiltonian is different for different n (in addition to being different for different l), so that only one of the N eigenvalues and eigenstates for each E_n^{C} has physical significance and the whole calculation has to be repeated to get another eigenvalue. If strong mixing of different n' were to occur in the expansion of ψ_{nlm}, Eq. (30), it would be difficult to identify this significant eigenstate. The results show, however, that this is no problem for all cases considered here, even near the continuum edge, since ψ^{C}_{nlm} always provides the largest contribution to ψ_{nlm}.

B. Debye potential as a test case

As a test of our method of approximation and especially of the truncated expansion of the wave function in terms of only a finite number of bound unperturbed hydrogen eigenstates (Sec. III A), we first computed the energy eigenvalues for a fictitious isolated hydrogen atom with a Debye (instead of the Coulomb) potential, i.e., omitting all other many-body effects in the wave equation (26). For this "isolated Debye atom," which is often considered as a model for hydrogen atoms in plasmas (e.g., [13,25,26] and references given there), Ref. [13] gives an extensive table of numerical results obtained in a completely different way by integrating the radial Schrödinger differential equation. Our calculations did reproduce all of these results (with the exception of a minor difference for one eigenvalue close to the continuum).

In particular, both approaches give identical results for the intersection of bound state energies with the continuum edge (which is invariably situated at zero energy in this case). At first sight, this is surprising for the approach used in this work since the perturbed states are constructed by superposition of only bound unperturbed states. However, the subspaces of bound and unbound states are different for the unperturbed atom and the atom in a plasma (the isolated Debye atom in the special case under discussion, but the argumentation obviously holds also for the more complicated cases treated here). Consider, for instance, a plasma density where all states except the $1s$ state have already merged into the continuum, so that the subspace of bound perturbed states is one-dimensional and all states that are orthogonal to ψ_{1s} are unbound perturbed states. Our numerical results show, for all plasma parameters investigated, that the perturbed state is always rather close to the unperturbed one $\psi_{1s} \approx \psi^{\mathrm{C}}_{1s}$, even near the continuum edge (for an example with dynamic screening, see Table I). But then, the bound unperturbed states $\psi^{\mathrm{C}}_{ns}(n = 2, 3, 4, \ldots)$, which are orthogonal to ψ^{C}_{1s}, are nearly orthogonal to ψ_{1s} and therefore must be superpositions mainly of unbound perturbed states. Moreover, to build the "wave packet" of the well-localized unperturbed $2s$ state, say, requires perturbed states from a broadband of continuous energies. This shows that our truncated basis of only *bound unperturbed* states does in fact contain a broad range of *unbound perturbed* states and therefore is appropriate to

investigate the merging of the bound perturbed nl state into the continuum provided the number N of unperturbed basis states is sufficiently larger than n (which can be tested by increasing the value of N).

From another point of view, the argumentation given above requires that the truncated basis of bound unperturbed states allows for the (approximate) identification of the continuum edge in the spectrum of perturbed eigenvalues. Since an N-dimensional basis yields only N discrete perturbed eigenvalues, this might indeed be impossible. Our results show, however, a quasicontinuum of closely spaced eigenvalues if N is larger than the number of bound states by about 6. Increasing N further adds more levels at the top of this group and decreases the interlevel distance at the bottom, but results in only minor changes of the position of the lowest level of the group. Therefore, this position can be taken as the position of the continuum edge, within an uncertainty given by the distance to the next higher level, and the plasma density at which a bound state merges into the continuum can be determined with corresponding uncertainty. Again, tests can be done (and the uncertainty can be diminished) by increasing the value of N.

In this way, the continuum edge for the isolated Debye atom was in fact found to be $E_{\rm cont} = 0$, the value known *a priori*. We also get agreement with Eq. (13) in the static limit for both the full and the classical dielectric function. For dynamic screening, things are slightly more involved, as discussed in Sec. IV B in connection with the numerical results.

C. Evaluation of matrix elements

The main numerical task in our approach is the evaluation of the matrix elements of the effective Hamiltonian in the basis of Coulomb states. With the three momentum integrals that appear in Eq. (6), the additional frequency integral in Eq. (7), and another three momentum integrals to obtain the matrix elements, these are originally given as sevenfold integrals. Using spherical coordinates for the momentum integrals, the two integrations over azimuth angles are trivial for a spherically symmetrical Hamiltonian. A third angle integration can be done analytically by standard methods based on the properties of angular momentum eigenstates, i.e., spherical harmonics. Then, we are left with a fourfold integral of a rather complicated integrand, the evaluation of which would require quite much computer time.

Therefore, we were lucky to be able to do the frequency integrals that occur in Eqs. (7) and (14) analytically [27,28]. In that part of these integrals which cannot be directly dealt with by applying the Kramers-Kronig relation for ε^{-1}, it is advantageous to extract the contributions from the pole at $\omega = \omega_0$ and the pole of the Bose function at $\omega = 0$ in the following way:

$$\mathrm{P}\int_{-\infty}^{+\infty}\frac{d\omega}{\pi}\frac{n_{\rm B}(\omega)}{\omega-\omega_0}\,\mathrm{Im}\,\varepsilon^{-1}(k,\omega) = \mathrm{Im}\int_{-\infty}^{+\infty}\frac{d\omega}{\pi}\left[\frac{n_{\rm B}(\omega)-n_{\rm B}(\omega_0)}{\omega-\omega_0}+\frac{1}{\hbar\beta\omega_0\omega}\right]\left[\frac{1}{\varepsilon(k,\omega)}-1\right]$$
$$+n_{\rm B}(\omega_0)\,\mathrm{P}\int_{-\infty}^{+\infty}\frac{d\omega}{\pi}\frac{\mathrm{Im}\,\varepsilon^{-1}(k,\omega)}{\omega-\omega_0}-\frac{1}{\hbar\beta\omega_0}\,\mathrm{P}\int_{-\infty}^{+\infty}\frac{d\omega}{\pi}\frac{\mathrm{Im}\,\varepsilon^{-1}(k,\omega)}{\omega}. \tag{31}$$

The last two integrals can immediately be evaluated using the Kramers-Kronig relation for ε^{-1}. The first integral on the rhs is no longer a principal value integral since its integrand has no poles on the real axis. This integral can be evaluated by closing the integration path with an infinite semicircle in the upper half of the complex ω plane and applying the residue theorem to the poles of the Bose function on the positive imaginary axis. [To get no contribution from the semicircle, $\mathrm{Im}\,\varepsilon^{-1}$ was replaced by $\mathrm{Im}(\varepsilon^{-1}-1)$ above.] As the result, we obtain

$$\mathrm{P}\int_{-\infty}^{+\infty}\frac{d\omega}{\pi}\frac{n_{\rm B}(\omega)}{\omega-\omega_0}\mathrm{Im}\,\varepsilon^{-1}(k,\omega)$$
$$= n_{\rm B}(\omega_0)\left[\mathrm{Re}\,\varepsilon^{-1}(k,\omega_0)-1\right]$$
$$-\frac{1}{\hbar\beta\omega_0}\left[\varepsilon^{-1}(k,0)-1\right]$$
$$-2\hbar\beta\omega_0\sum_{j=1}^{\infty}\frac{\varepsilon^{-1}\left[k,i\,2\pi j/(\hbar\beta)\right]-1}{(\hbar\beta\omega_0)^2+(2\pi j)^2} \tag{32a}$$

$$= n_{\rm B}(\omega_0)\left[\mathrm{Re}\,\varepsilon^{-1}(k,\omega_0)-1\right]$$
$$-\sum_{j=-\infty}^{\infty}\frac{\varepsilon^{-1}\left[k,i\,2\pi j/(\hbar\beta)\right]-1}{\hbar\beta\omega_0+i\,2\pi j}, \tag{32b}$$

where $\varepsilon(k,\omega) = \varepsilon^*(k,-\omega)$ is real for purely imaginary frequencies. The large-j "tail" of the infinite series can be added up by utilizing the high-frequency asymptotic expansion of ε^{-1}, so that only a finite number of terms have to be evaluated numerically.

The integral given above is often encountered in Green-function theory of charged particle systems and was commonly calculated by use of a (single or double) plasmon-pole approximation or a rational approximation for $\mathrm{Im}\varepsilon^{-1}$ in previous work (e.g., [4,12,29,7]). With Eq. (32), these approximations can be avoided. As another example of its usefulness, we note that application of Eq. (32b) in Eq. (11) directly recovers a result for the retarded one-particle self-energy, which was recently obtained [30] by explicit construction of the analytic contin-

uation of the self-energy from the imaginary Matsubara frequencies (for which it is originally defined) to the complex frequency plane.

We emphasize that the validity of Eq. (32a) is not restricted to the RPA dielectric function because its derivation is based on general principles such as the Kramers-Kronig relation for ε^{-1} (i.e., causality arguments applied to the formation of the polarization cloud, which screens an electric charge in a plasma).

In our case, the resonance frequency ω_0 is a function of momentum q, say, and Eq. (32a) transforms a double integral over the momentum-frequency plane into a single integral along some curve in this plane. $\mathrm{Re}\varepsilon^{-1}$ is sharply peaked in the immediate vicinity of another curve, the "plasmon-pole curve" given by $\mathrm{Re}\varepsilon(q/\hbar,\omega)=0$ in combination with small $\mathrm{Im}\varepsilon$. If the two curves intersect, the numerical momentum integration has to be done particularly carefully. In the work reported here, the numerical integration routine did an extra search for this intersection, but never found one for the atomic and plasma parameters investigated.

Finally, we annotate that only one integral has to be evaluated numerically to calculate the effective Hamilton matrix in the static limits for the full and the classical dielectric function.

IV. RESULTS AND DISCUSSION

We did rather extensive numerical computations for the continuum edge and bound states from $1s$ to $4f$ for $\beta = 1/(k_\mathrm{B}T) = 1$, 2, 4, 8, and 16 Ry^{-1} [31] (corresponding to temperatures T of about 160 000 K, 80 000 K, 40 000 K, 20 000 K, and 10 000 K), with the plasma density ranging from very low values up to and beyond the value where the Mott transition of the $1s$ state takes place. We note that our high-density results for the lower of these temperatures are uncertain because the plasma becomes degenerate (and our approximations cease to be valid) in the vicinity of the Mott transition density.

The computations were done for the dynamic classical and full dielectric functions and their static limits by considering the following four cases: static screening; namely, (i) Eq. (24), the (classical) Debye approximation $\varepsilon_\mathrm{D}(k)$, together with wave equation (26) and Eq. (27) for the continuum edge ("Debye limit"), and (ii) Eq. (23), the static limit of the full RPA dielectric function $\varepsilon_\mathrm{st}(k)$ (including additional quantum corrections), together with the appropriate static limits of the general wave equation (6) and of Eq. (13) for the continuum edge ("static full screening"); and dynamic screening [in Eq. (7) for $\Delta V_{ie}^\mathrm{eff}$, to be used in the effective wave equation (6) and in Eq. (14) for the corresponding continuum edge], namely, (iii) the classical RPA dielectric function $\varepsilon_\mathrm{cl}(k,\omega)$, Eq. (22) ("dynamic classical screening"), and (iv) the full RPA dielectric function $\varepsilon(k,\omega)$, Eq. (19) ("dynamic full screening").

As a general observation, the hydrogenic energy levels in a plasma remain practically unshifted if the plasma density is increased at constant temperature and show a stronger downward shift only near the crossover with the lowered continuum edge. The weak density dependence results from compensation of opposite shifts caused by the different many-particle effects, as discussed in Refs. [4,12,20]. The compensation takes place between the Pauli blocking and the Hartree-Fock self-energy and between the dynamically screened effective potential correction and the dynamic (Montroll-Ward) self-energy. While the (negative) self-energies lead to a lowering of the energy levels, Pauli blocking and screening reduce the atomic ion-electron interaction and lead to an increase of the levels. With increasing density, the self-energies start to dominate and eventually produce the stronger decrease of energy levels near the intersection with the continuum edge. This behavior is found for all levels, but already at lower densities for higher excited levels.

For the continuum edge, no such compensation is effective since it is determined by the self-energies alone, according to Eq. (13). Therefore, the continuum edge decreases more steeply with increasing density than the bound energy levels and these merge into the continuum one by one in order of decreasing main quantum number n. Finally, even the $1s$ ground state energy level crosses the continuum edge, which is known as the Mott transition. Beyond the Mott transition, bound states cease to exist in a hydrogen plasma.

A. Static screening

We first investigated the hydrogen energy levels for static screening, where calculations are less involved than for dynamic screening and some results for the Debye limit are already available [16]. In the static case, the energy eigenvalues are real and there is no damping or level broadening.

Results for two temperatures are compared in Fig. 1 for the $1s$ and $2s$ states, respectively, and the continuum edge. The continuum-edge curves shown in the figures were computed according to the static limit of Eq. (13) [i.e., Eq. (27) for the Debye limit]. The continuum edge was also determined from the quasicontinuum solutions of the static limit of the effective wave equation, as discussed in Sec. III B, and perfect coincidence was found within our numerical accuracy. For static full screening, case (ii), the energy-level shifts are slightly smaller than those for Debye screening, case (i), the differences being more pronounced at the lower temperature.

B. Dynamic screening

In the calculations for dynamic screening, the approximations discussed in Sec. II B were made, i.e., the quasiparticle energies were replaced by the kinetic energies and $\hbar\omega$ was replaced by the unperturbed Coulomb eigenvalues E_n^C in the effective Hamiltonian, but E_cont was self-consistently determined by iteration.

With static screening, the effective Hamiltonian does not depend on the perturbed eigenvalue and its diagonalization gives, at any density, a whole set of energies for bound and quasicontinuum states at once. In contrast, the effective Hamiltonian for dynamic screening, calcu-

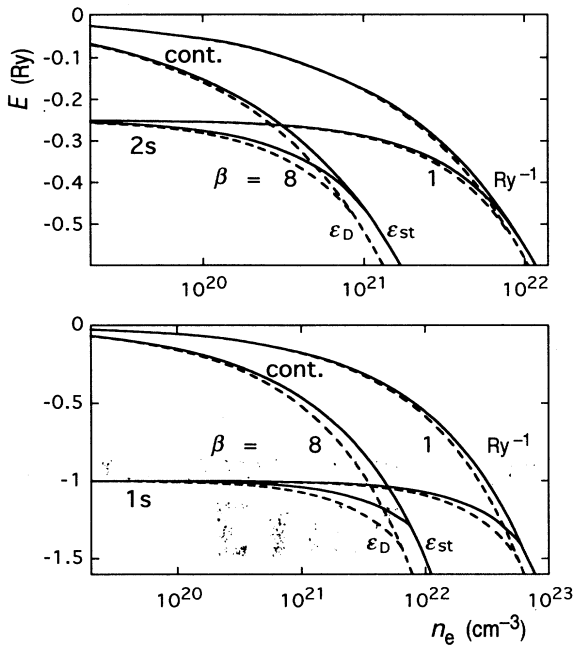

FIG. 1. Energies E of the continuum edge (cont.) and the $1s$ and $2s$ bound states as functions of the electron density n_e for static screening. Solid lines, static limit ε_{st} of the full dielectric function (with quantum corrections), case (ii); broken lines, static Debye limit ε_D of classical dielectric function, case (i). Results are shown for $\beta = 1\,\mathrm{Ry}^{-1}$ ($\beta^{-1} = k_B T \approx 13.6\,\mathrm{eV}$, $T \approx 157\,900$ K) and $\beta = 8\,\mathrm{Ry}^{-1}$ ($k_B T \approx 1.7$ eV, $T \approx 19\,740$ K).

lated with $\hbar\omega = E_n^C$, yields only one perturbed eigenvalue $E_{nl} = \hbar\omega_{nl} \approx E_n^C$, while its other eigenvalues have no physical significance. The only exception would be another energy level with $E_{n'l} = E_{nl}$. According to our numerical results, no such level crossing occurs between bound perturbed states. However, if the bound state under consideration merges into the quasicontinuum as the plasma density is increased, a level crossing takes place with the lowest of the quasicontinuum energy levels, so that the continuum edge can be determined at that particular density. As a typical example, Table I presents the perturbed $1s$ state and the two lowest-lying of the quasicontinuum states [with the expansion according to Eq. (30) done up to $n' = 10$] for $\beta = 2\,\mathrm{Ry}^{-1}$ at densities clearly below, slightly below, and slightly above the Mott transition density, which correspond to $\kappa a_0 = 0.5$, 0.6, and 0.65, respectively ($a_0 \approx 53$ pm Bohr radius). It is obviously no problem to identify the two different types of states.

In Figs. 2 and 3, which show some of our results, bound energy levels are always drawn up to this density where they merge into the continuum. These end points should lie on the curve for the continuum edge, but are always found to be slightly below (with dynamic screening). This is due to the different treatment of $E = \hbar\omega$ for bound states or the continuum edge, as shown by test calculations we did for some plasma densities and temperatures. On the one hand, we did not replace $\hbar\omega$ by E_n^C for the nl bound state, but extended our calculations to determine the self-consistent solution $\hbar\omega = E_{nl}$; this did bring the end points of the bound-level curves up onto the continuum-edge curve. On the other hand, we formally replaced E_{cont} by E_n^C in the calculation of continuum curves [rhs of Eq. (14)]. This brought the continuum curves down to the end points of the bound-level curves in the figures (but cannot be used for lower and higher densities). Thus there is no indication in the frame of our approximations that Eq. (13) might not yield the correct continuum edge, contrary to conclusions drawn in the frame of different approximations [7].

Figure 2 presents the energies of the $1s$ and $2s$ states and of the continuum edge as functions of plasma density, at fixed temperatures of about 160 000 K and 20 000 K, for approximations (ii) and (iv), i.e., the static and the dynamic full dielectric function. Inspection of this figure

TABLE I. Perturbed $1s$ state and lowest-lying quasicontinuum states for plasma densities clearly below, slightly below, and slightly above the Mott density [$\beta = 2\,\mathrm{Ry}^{-1}$, full dynamic RPA dielectric function, case (iv)]. Perturbed states are approximated as linear combinations $c_1\psi_{1s}^C + \cdots + c_{10}\psi_{10s}^C$ of unperturbed Coulomb states; cf. Eq. (30).

E (Ry)	c_1	c_2	c_3	c_4	c_5	c_6	c_7	c_8	c_9	c_{10}
$\kappa = 0.5a_0^{-1}$, $n_e = 1.68 \times 10^{22}$ cm^{-3}										
−0.9157	0.0003	0.0039	−0.0168	0.0687	−0.1952	0.4175	−0.5958	0.4344	0.2336	−0.4293
−0.9185	−0.0002	−0.0000	−0.0041	0.0087	−0.0318	0.0763	−0.2162	0.4662	−0.7084	0.4767
−1.0908	0.9811	−0.1875	−0.0337	−0.0215	−0.0155	−0.0121	−0.0099	−0.0086	−0.0076	−0.0068
$\kappa = 0.6a_0^{-1}$, $n_e = 2.42 \times 10^{22}$ cm^{-3}										
−1.1024	0.0002	−0.0022	0.0077	−0.0401	0.1342	−0.3539	0.5934	−0.5045	−0.1994	0.4568
−1.1059	0.0017	−0.0009	−0.0032	0.0056	−0.0236	0.0596	−0.1919	0.4522	−0.7180	0.4890
−1.1341	0.9439	−0.3270	0.0139	−0.0280	−0.0172	−0.0143	−0.0122	−0.0122	−0.0121	−0.0137
$\kappa = 0.65a_0^{-1}$, $n_e = 2.84 \times 10^{22}$ cm^{-3}										
−1.1644	0.8104	−0.4393	0.1970	0.0082	−0.2268	−0.1410	0.0174	0.1082	0.1296	0.1057
−1.1984	0.0007	0.0015	−0.0054	0.0311	−0.1119	0.3268	−0.5871	0.5345	0.1794	−0.4659
−1.2023	0.0012	−0.0001	0.0026	−0.0056	0.0248	−0.0562	0.1804	−0.4396	0.7215	−0.4998

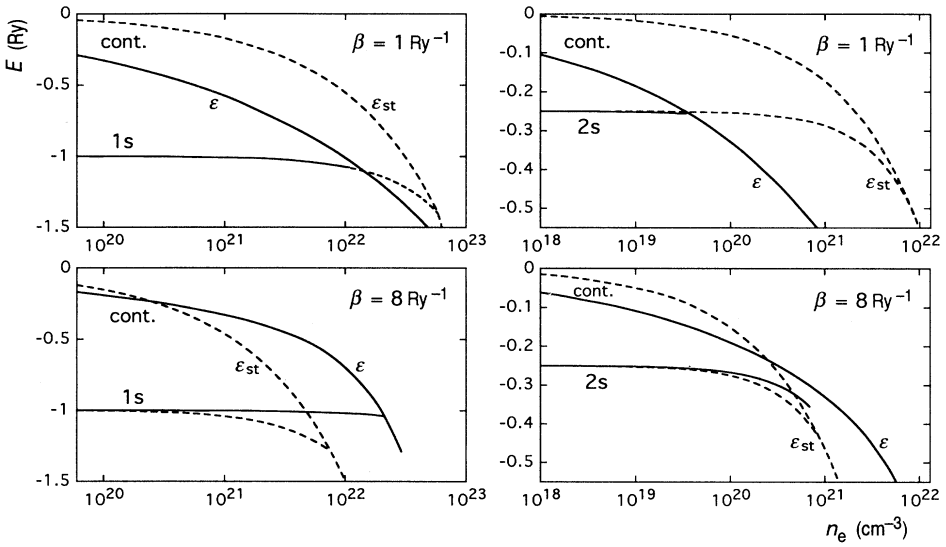

FIG. 2. Energies E of the continuum edge (cont.) and the $1s$ and $2s$ bound states as functions of electron density n_e for dynamic and static screening. Solid lines, full dynamic RPA dielectric function ε, case (iv); broken lines, corresponding static limit ε_{st}, case (ii). Results are shown for $\beta = 1\,\mathrm{Ry}^{-1}$ and $\beta = 8\,\mathrm{Ry}^{-1}$.

(and of the other data we computed) shows that there is no simple characterization of the differences between the effects of static and dynamic screening, which depend on plasma density and temperature as well as the main quantum number n, concerning not only their magnitude but also their sign. As an example, the Mott density (where the $1s$ state merges into the continuum) is larger with static screening than with dynamic screening at $T = 160\,000$ K, but smaller at $T = 20\,000$ K (Fig. 2).

The general conclusion to be drawn from these results is that the effects of dynamic screening have to be included in reliable calculations of the plasma effects on atomic structure. The use of static screening greatly facilitates calculations, but may lead to substantial errors (cf. Fig. 2 and Table II, for example). However, even if our results emphasize the importance of dynamic screening, they indicate as well that the corresponding more complicated calculations can probably be done very accurately by low-order perturbation theory [32,33] for the bound states since the perturbed states remain close to the unperturbed ones even near the Mott density.

As compared to the differences of static vs dynamic screening, the differences brought about by use of the dynamic classical instead of the dynamic full dielectric function, cases (iii) and (iv) above, are small and similar to the differences found between the corresponding static limits: the full dielectric function, with quantum effects included, leads to slightly smaller level shifts, with somewhat larger effects at lower temperatures. As a qualitative difference of these two cases at high plasma densities, the $1s$-level shift is smaller for higher than for lower temperatures with classical screening, while this order is reversed with full screening [34].

At low plasma densities, where perturbation theory [32,33] is certainly appropriate, the level shifts are found to be proportional to κ^2,

$$E_{nl} - E_n^{\mathrm{C}} = -\alpha_{nl}\,\frac{1}{2}\,\frac{e^2\,a_0}{4\pi\varepsilon_0}\,\kappa^2 = -\alpha_{nl}\,a_0^2\,\kappa^2\,\mathrm{Ry}, \qquad (33)$$

i.e., they are proportional to the density at fixed temperature. In Table II, the coefficients α_{nl} for some hydrogen energy levels are given, as found for approximations (i)–(iv). These data also exemplify the conclusions stated above.

We emphasize that Eq. (33) holds for neutral hydrogen *atoms*. In contrast, *level* shifts for hydrogenlike *ions* such as He II are expected to be proportional to κ at low densities [35,36]. However, this lowest-order contribution to the level shifts is the same for all bound states because it is the self-energy shift experienced by the ion as a whole (due to its net electrical charge) on immersion in a plasma. Therefore, this contribution cancels if line shifts are calculated as level shift differences, so that *line* shifts are in general found to be proportional to the plasma density (i.e., κ^2) for both hydrogenlike ions and hydrogen atoms.

For dynamic full screening, case (iv), Fig. 3 shows the energies E for the $1s$ and $2p$ states and the continuum edge as functions of κ (instead of n_e) for different temperatures. This kind of representation would be fully appropriate for the model of the isolated Debye atom (Sec. III B), for which all density and temperature dependence enters through κ. For cases (i) and (ii), i.e., static screening inclusive of the additional many-particle effects, the corresponding curves for different temperatures are still found to be practically coincident, with slightly larger high-density level shifts for lower than for higher temperatures. The large spread with temperature of the curves in Fig. 3 demonstrates the additional temperature dependence that is brought about by dynamic screening. With dynamic full screening, the level shifts (in particular the shifts of the continuum edge) for different temperatures are distinctly different at fixed κ and they are larger for higher than for lower temperatures.

The imaginary parts Γ of the bound state energies, which give the decay rates (damping) due to interaction with the surrounding plasma, are also shown in Fig. 3. They are found to be small throughout (so that their

TABLE II. Factors of proportionality α_{nl} according to Eq. (33), $E_{nl} - E_n^C = -\alpha_{nl} a_0^2 \kappa^2$ Ry, for the four investigated levels of approximation of the RPA dielectric function: (i) static Debye screening ε_D, $\hbar \to 0$ and $\omega \to 0$; (ii) static full screening ε_{st}, $\omega \to 0$; (iii) classical dynamic screening ε_{cl}, $\hbar \to 0$; and (iv) full dynamic screening ε. Range of validity $\kappa \lesssim 10^{-4} a_0^{-1}$.

			Case			
β (Ry^{-1})	T (K)	nl	(i) ε_D	(ii) ε_{st}	(iii) ε_{cl}	(iv) ε
		$1s$	1.482	1.169	1.276	1.097
1		$2s$	6.319	5.905	25.30	24.87
	157 900	$2p$	5.273	4.867	17.72	17.31
		$4f$	18.43	18.00	237.1	236.6
		$1s$	1.446	1.058	0.6561	0.4931
2		$2s$	6.266	5.699	13.83	13.31
	78 950	$2p$	5.205	4.649	9.684	9.220
		$4f$	18.40	17.79	129.9	129.3
		$1s$	1.439	0.9751	0.3448	0.2064
4		$2s$	6.201	5.438	7.407	6.866
	39 470	$2p$	5.142	4.400	5.197	4.723
		$4f$	18.35	17.49	70.46	69.46
		$1s$	1.451	0.9132	0.1999	0.082 80
8		$2s$	6.127	5.118	3.916	3.409
	19 740	$2p$	5.092	4.127	2.763	2.340
		$4f$	18.29	17.09	37.13	36.23
		$1s$	1.468	0.8617	0.1316	0.032 99
16		$2s$	6.058	4.759	2.091	1.658
	9870	$2p$	5.060	3.849	1.516	1.156
		$4f$	18.21	16.57	19.28	18.19

calculation by means of perturbation theory is justified *a posteriori*), with a rather steep increase of magnitude just before the bound state merges into the continuum.

Finally, the Mott density, at which the $1s$ state merges into the continuum, is shown as a function of temperature in Fig. 4. For cases (i) and (ii) with static screening, there are only small deviations from the result found for the isolated Debye atom [13], where the Mott transition occurs at a Debye length of

$$r_D^{\text{Mott}} \approx 0.84 a_0 \tag{34}$$

and the Mott density is proportional to the temperature (straight line in Fig. 4). In contrast, the Mott density with dynamic full screening, case (iv), has a maximum at a temperature of about 50 000 K and decreases with further increasing temperature. As we did only investigate temperatures up to 160 000 K, we cannot decide whether the Mott density continues to decrease at still higher temperatures or eventually starts to increase again.

As set forth in Sec. III C, our calculations with dynamic screening could be done without the introduction of another approximation for $\text{Im}\varepsilon^{-1}$ in order to obtain an analytical result for the frequency integral in Eq. (7). In

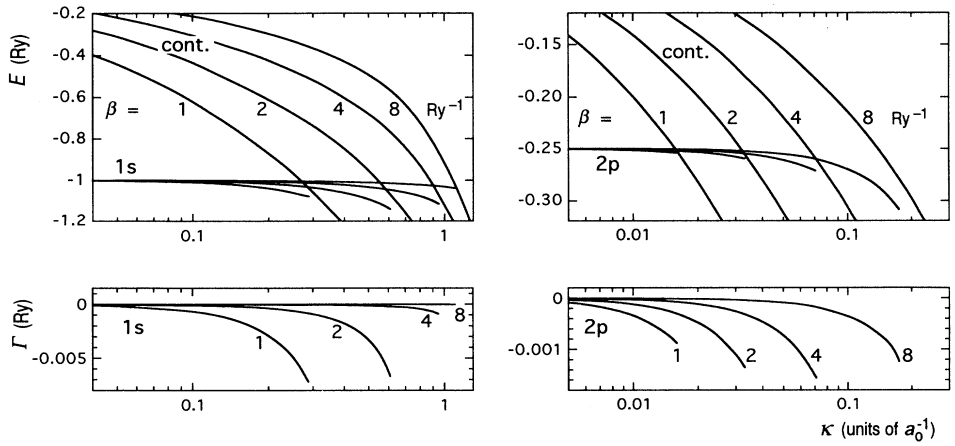

FIG. 3. Energies E of the continuum edge and the $1s$ and $2p$ bound states for full dynamic screening ε, case (iv), at $\beta = 1$, 2, 4, and 8 Ry^{-1} (with corresponding numbering of curves). Below the real parts E, the imaginary parts Γ of the bound state energies are shown on an enlarged energy scale. Results are presented as functions of the inverse Debye length $\kappa = 1/r_D = \sqrt{2n_e\beta e^2/\varepsilon_0}$, measured in units of the inverse Bohr radius a_0.

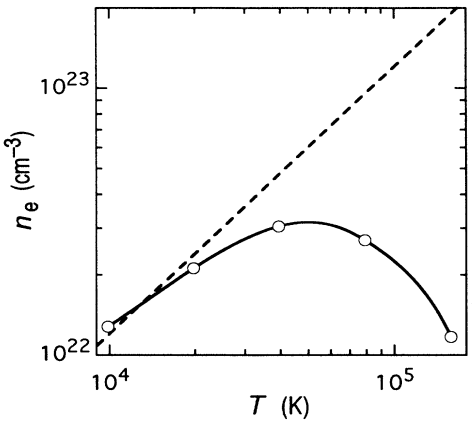

FIG. 4. Mott density (where the $1s$ state merges into the continuum) as a function of temperature. Solid line, full dynamic RPA dielectric function ε, case (iv); broken line, Mott condition Eq. (34).

Ref. [29], a double plasmon-pole approximation was employed for this purpose. Comparing corresponding low-density results, this approximation is found to work quite well for excited levels since it yields level shifts that do not deviate by more than some 10% from the shifts calculated here [34]. For the $1s$ level, which is much less shifted, we obtain only about one-half the shift found in Ref. [29].

Concerning comparison with experiment, direct measurements of the *level* shifts and widths calculated here are not available since they would have to be done relative to some energy level of an unperturbed atom, the continuum edge of which defines energy zero. However, differences of perturbed energies can be measured as spectral line shifts (and sums of the imaginary parts of energies as linewidths) if the vertex contributions (interference terms) mentioned in the Introduction are not too important, which account for statistically correlated perturbations of the upper and lower level of a spectral line. They are least important for the Lyman lines $np \leftrightarrow 1s$ because the $1s$ state is much more tightly bound than the excited states. This is also shown by our results, which predict a $1s$ shift that is only a few percent of the np shifts at low plasma densities (Table II). Since both shifts are toward lower energies, our results predict redshifts of the Lyman lines, proportional to the plasma density at low densities. This is in accordance with the measured shifts. However, the calculated shifts are an order of magnitude larger than the measured ones [37–39]. Moreover, the measured Lyman line shifts are a few percent at most of the measured widths, while the calculated imaginary parts of the energy eigenvalues are distinctly smaller than the real parts. Disregarding the vertex contributions, the situation is similar for the Balmer lines [40–44].

Thus we are forced to conclude that one or more of the approximations we used are not reliable. One of these might be the approximation of the effective two-particle interaction K_{ie} by the screened potential V_{ie}^s, Eq. (2). As a result of this, the effective potential correction $\Delta V_{ie}^{\text{eff}}$ is found to be caused by plasmon-induced virtual bound-free transitions [resonance denominator of Eq. (7) combined with the plasmon peak of $\text{Im}\varepsilon^{-1}$], while virtual bound-bound transitions are not included. However, calculations employing the double plasmon-pole approximation show [29] that their inclusion in $\Delta V_{ie}^{\text{eff}}$ leads to still larger calculated line shifts and does not remove, but even increases, the discrepancies with experiment.

Therefore, we believe that the discrepancies are mainly due to an inappropriate treatment of the ion contribution to the electronic self-energy, which is very large in the RPA for $m_i \gg m_e$ [4,15] and small momentum, and probably requires an improved approximation. We note that spectral line broadening calculations [45] restrict the Green-function treatment to plasma electrons for this reason and employ a statistical ion microfield distribution (with corresponding static Stark splitting of energy levels) for the ion contribution. This split approach is not able, however, to account for thermal ion motion ("ion dynamic effects").

V. CONCLUSIONS

In this work, we determined two-particle (hydrogen-atom) states in an equilibrium hydrogen plasma by solving the effective wave equation, which can be derived from the Bethe-Salpeter equation by means of the quantum statistical Green-function technique. In this wave equation, the influence of the plasma is taken into account in terms of the Hartree-Fock and dynamic Montroll-Ward self-energies, Pauli blocking factors, and a dynamic effective correction of the Coulomb interaction potential. The main approximations used in its derivation are a screened-ladder approximation by taking the effective ion-electron interaction kernel K_{ie} to be the dynamically screened potential V_{ie}^s, Eq. (2), and the Shindo approximation, Eq. (4), to replace a two-frequency Green function by a single-frequency one. In correspondence to the first approximation, we also neglected contributions to the single-particle self-energies beyond the Montroll-Ward contribution [the V^s approximation, Eq. (10)]. Plasma-specific effects are incorporated into the effective wave equation through the plasma dielectric function that we used in the RPA, Eq. (17).

The resulting atomic "plasma Hamiltonian" being non-Hermitian, atomic states in a plasma have complex energies and are no longer stationary, but decay. To determine these energies, we first calculated eigenvectors and real eigenvalues of the Hermitian part of the Hamiltonian according to Eq. (6), neglecting higher-order density contributions (except those contained in the dielectric function) and considering only the case of an atom with zero center-of-mass momentum. Then we used these numerical results to determine the imaginary parts of the energies by perturbation theory. With an analytical result Eq. (32) for the frequency integrals that occur in the effective potential correction Eq. (7), we could do the calculations with the full dynamic RPA dielectric function (or its classical limit) and avoid the plasmon pole or

rational approximations employed in previous work. For comparison, we also determined the real energies resulting from static screening.

Our calculations show that there are distinct differences between the results obtained with static and with dynamic screening, in particular with respect to the temperature dependence of energy level shifts and to the Mott densities, where the $1s$ state merges into the continuum. In general, the effects of dynamic screening therefore have to be included in reliable calculations of the plasma effects on atomic structure. Dynamic screening leads to more effective compensation between self-energy and screening effects, so that level shifts are smaller than for static screening. As a consequence of our approximations, the dynamic effective potential correction is due only to plasma induced virtual bound-free transitions, while the corresponding contribution of bound-bound transitions is missing and should be included into an improved calculation.

Calculated shifts of the first Lyman and Balmer spectral lines are much larger than the measured shifts, and also larger than the calculated widths, contrary to experimental results. We attribute this to an overestimate of the ion contribution to the electronic self-energy for large ion-to-electron mass ratios. In this regard, consistent further improvement of the Green-function approach is required.

ACKNOWLEDGMENTS

This work was in part supported by the BMFT of Germany. One of us (S.A.) would like to thank PTB for the hospitality shown during a stay when this work was initiated.

[1] *Strongly Coupled Plasma Physics*, edited by F. J. Rogers and H. E. DeWitt (Plenum, New York, 1987); *Strongly Coupled Plasma Physics*, edited by S. Ichimaru (Elsevier, Tokyo, 1990); *Strongly Coupled Plasma Physics*, edited by H. M. Van Horn and S. Ichimaru (University of Rochester Press, Rochester, 1993).

[2] L. P. Kadanoff and G. Baym, *Quantum Statistical Mechanics* (Benjamin, New York, 1962).

[3] W. Ebeling, W. D. Kraeft, and D. Kremp, *Theory of Bound States and Ionization Equilibrium in Plasmas and Solids* (Akademie-Verlag, Berlin, 1976).

[4] W. D. Kraeft, D. Kremp, W. Ebeling, and G. Röpke, *Quantum Statistics of Charged Particle Systems* (Akademie-Verlag, Berlin, 1986).

[5] K. Kilimann, D. Kremp, and G. Röpke, Teor. Mat. Fiz. **55**, 448 (1983).

[6] G. Röpke, K. Kilimann, D. Kremp, W. D. Kraeft, and R. Zimmermann, Phys. Status Solidi B **88**, K59 (1978).

[7] W. Schäfer, R. Binder, and K. H. Schuldt, Z. Phys. B **70**, 145 (1988).

[8] T. Seifert, Ph.D. thesis, University of Rostock, 1981 (unpublished).

[9] R. Zimmermann, Phys. Status Solidi B **48**, 603 (1971).

[10] R. Zimmermann, Phys. Status Solidi B **76**, 191 (1976).

[11] R. Zimmermann, *Many-Particle Theory of Highly Excited Semiconductors* (Teubner, Leipzig, 1988).

[12] R. Zimmermann, K. Kilimann, W. D. Kraeft, D. Kremp, and G. Röpke, Phys. Status Solidi B **90**, 175 (1978).

[13] F. J. Rogers, H. C. Graboske, Jr., and D. J. Harwood, Phys. Rev. A **1**, 1577 (1970).

[14] K. Kilimann (unpublished).

[15] W. D. Kraeft, B. Strege, and M. D. Girardeau, Contr. Plasma Phys. **30**, 563 (1990).

[16] W. D. Kraeft, D. Kremp, K. Kilimann, and H. E. DeWitt, Phys. Rev. A **42**, 2340 (1990).

[17] K. Shindo, J. Phys. Soc. Jpn. **29**, 287 (1970).

[18] K. Kilimann and W. D. Kraeft, Mitteilungen des Zentralinstituts für Isotopenforschung der Akademie der Wissenschaften der DDR **13**, 70 (1978).

[19] D. Klähn and K. Kilimann, Phys. Status Solidi B **77**, 483 (1976).

[20] K. Kilimann, W. D. Kraeft, and D. Kremp, Phys. Lett. **61A**, 393 (1977).

[21] Yu. L. Klimontovich and W. D. Kraeft, Teplofiz. Vys. Temp. **12**, 239 (1974) [High Temp. (USSR) **12**, 212 (1975)].

[22] W. Gautschi, in *Handbook of Mathematical Functions*, edited by M. Abramowitz and I.A. Stegun (Dover, New York, 1965).

[23] G. Ecker and W. Weizel, Ann. Phys. (Leipzig) **17**, 126 (1956).

[24] H. A. Bethe and E. E. Salpeter, *Quantum Mechanics of One- and Two-Electron Atoms* (Springer, Berlin, 1957).

[25] D. Singh and Y. P. Varshni, Phys. Rev. A **29**, 2895 (1984).

[26] F. A. Gutierrez, H. Jouin, and E. Cormier, J. Quant. Spectrosc. Radiat. Transfer **51**, 665 (1994).

[27] B. Strege, Ph.D. thesis, University of Greifswald, 1990 (unpublished).

[28] J. Seidel and S. Arndt (unpublished).

[29] G. Röpke, T. Seifert, and K. Kilimann, Ann. Phys. (Leipzig) **38**, 381 (1981).

[30] Ben Yu-Kuang Hu and S. Das Sarma, Phys. Rev. B **48**, 5469 (1993).

[31] All equations are written in dimensionally correct form, independent of units. For the presentation of results, we adopt common practice and use atomic units to facilitate the comparison with other work. Thus the ionization energy of ground-state hydrogen atoms (one-half the Hartree energy) is used as unit of energy and denoted as $1\,\mathrm{Ry} = e^2/(8\pi\varepsilon_0 a_0) \approx 13.6\,\mathrm{eV}$. The Bohr radius $a_0 \approx 53\,\mathrm{pm}$ is the atomic unit of length.

[32] S. Arndt, T. Bornath, W. D. Kraeft, and J. Seidel, in *XX International Conference on Phenomena in Ionized Gases, Contributed Papers*, edited by V. Palleschi and M. Vasselli (Istituto di Fisica Atomica e Molecolare, Pisa, 1991), Vol. 4, p. 863.

[33] R. Fehr and W. D. Kraeft, Phys. Rev. E **50**, 463 (1994)

[34] S. Arndt, Ph. D. thesis, University of Greifswald, 1993 (unpublished).
[35] G. Röpke, K. Kilimann, D. Kremp, and W. D. Kraeft, Phys. Lett. **68A**, 329 (1978).
[36] W. Ebeling and K. Kilimann, Z. Naturforsch. Teil A **44**, 519 (1988).
[37] K. Grützmacher and B. Wende, Phys. Rev. A **18**, 2140 (1978).
[38] M. Geisler, K. Grützmacher, and B. Wende, in *Spectral Line Shapes*, edited by B. Wende (de Gruyter, Berlin, 1981), p. 103.
[39] K. Gruetzmacher and B. Wende, in *Spectral Line Shapes,* edited by R. J. Exton (Deepak, Hampton, 1987), p. 59.
[40] W. L. Wiese, D. E. Kelleher, and D. R. Paquette, Phys. Rev. A **6**, 1132 (1972).
[41] J. Halenka and J. Musielok, J. Quant. Spectrosc. Radiat. Transfer **36**, 3 (1986).
[42] H. R. Griem, Phys. Rev. A **38**, 2943 (1988).
[43] S. Djurovic, Z. Mijatovic, and R. Kobilarov, Contr. Plasma Phys. **28**, 229 (1988).
[44] J. Halenka, Z. Phys. D **16**, 1 (1990).
[45] S. Günter, L. Hitzschke, and G. Röpke, Phys. Rev. A **44**, 6834 (1991).